THE JOURNAL OF PHYSICAL CHEMISTRY C

Article

pubs.acs.org/JPCC

Directionality of Ultrafast Electron Transfer in a Hydrogen Evolving Ru−Pd-Based Photocatalyst

Qing Pan,[†] Francesco Mecozzi,[‡] Jeroen P. Korterik,[†] Divya Sharma,[†] Jennifer L. Herek,[†] Johannes G. Vos,[§] Wesley R. Browne,[‡] and Annemarie Huijser*[,†]

[†]Optical Sciences group, MESA+ Institute for Nanotechnology, University of Twente, P.O. Box 217, 7500 AE, Enschede, The Netherlands

[‡]Stratingh Institute for Chemistry, Faculty of Mathematics and Natural Sciences, University of Groningen, Nijenborgh 4, 9747 AG, Groningen, The Netherlands

[§]SRC for Solar Energy Conversion, School of Chemical Sciences, Dublin City University, Glasnevin, Dublin 9, Ireland

Supporting Information

ABSTRACT: Directionality of electron transfer and long-lived charge separation are of key importance for efficient photocatalytic water splitting. Knowledge of the processes that follow photoexcitation is essential for the optimization of supramolecular assembly designs in order to improve the efficiency of photocatalytic hydrogen generation. Photoinduced intramolecular electron transfer processes within the hydrogen-evolving photocatalyst $[Ru(bpy)_2(tpy)Pd(CH_3CN)Cl]^{2+}$ (**RuPd**; bpy = bipyridine, tpy = 2,2′:5′,2″-terpyridine) have been studied by resonance Raman, femtosecond transient absorption, and time-resolved photoluminescence spectroscopies. Comparison of the photophysical properties of **RuPd** with those of the mononuclear precursor $[(bpy)_2Ru(tpy)]^{2+}$ (**Ru**) enables establishment of a photophysical model ranging from the femtosecond to the submicrosecond domain. Optical excitation of **Ru** and **RuPd** populates both bpy- and tpy-based ^{1}MLCT (metal-to-ligand charge transfer) singlet states, from where intersystem crossing (ISC) into corresponding ^{3}MLCT triplet states occurs. Electron density localized on the peripheral bpy ligands can subsequently flow to the tpy bridging ligand by interligand electron transfer, which process occurs with a time constant of 32.5 (±1.5) ps for **RuPd**. Not all electron density undergoes this process, most likely due to a competing loss channel on the bpy ligand caused by vibrational relaxation occurring at a time scale of 9.1 (±0.4) ps. The relaxed $^3MLCT_{bpy}$ and $^3MLCT_{tpy}$ states have excited state lifetimes of 400 (±1) ns and 88 (±1) ns, respectively. Electron transfer from the tpy ligand to Pd may take place on a ∼100 ns time scale, but it is also possible that the final relaxed excited state is delocalized over the tpy ligand and the Pd center. The insight that optical excitation populates both the peripheral bpy ligands and the bridging tpy ligand, and that part of the electron density subsequently flows from the former to the latter, is important for the realization of efficient photocatalytic hydrogen generation. The next step is to make the interligand electron transfer process faster, by functionalizing the peripheral ligands with electron-donating moieties, and adapting the nature of the bridging ligand and the catalytic metal center.

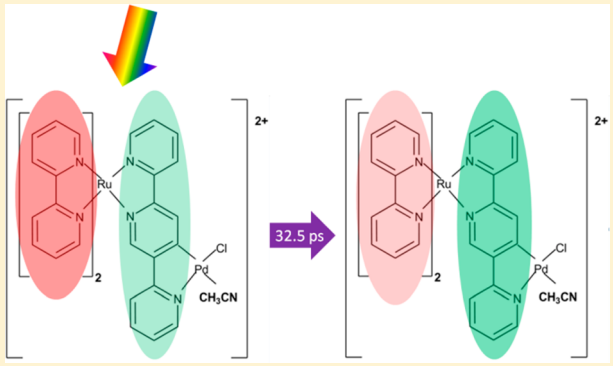

INTRODUCTION

The photocatalytic splitting of water into hydrogen and oxygen is a primary target in producing renewable green fuel and storing transient energy sources such as wind and solar energy.[1] Splitting of water requires the transfer and accumulation of multiple electrons, and hence, in synthetic systems, directional electron transfer and long-lived charge separation are required. The search for molecular candidates has focused on ruthenium(II) polypyridyl based complexes, with $[Ru(bpy)_3]^{2+}$ serving as a starting point for a supramolecular and multicomponent approach to hydrogen generation, in large part due to the ultrafast intersystem crossing (ISC), long-lived excited states, and chemical stability with regard to both reversible oxidation and reduction.[2−5]

In the case of the reduction of protons to hydrogen, one approach is to physically mix the light-absorbing photosensitizer and catalytic center, in the presence of a sacrificial electron donor such as triethylamine (TEA) to regenerate the photosensitizer after photoinduced electron transfer to a catalytic center, where proton reduction takes place. A drawback of this intermolecular approach is that the electron transfer from the photosensitizer to the catalytic center is diffusion limited.[6] An alternative approach involves the use of intramolecular charge transfer processes. In this approach, the

Received: June 24, 2014
Revised: August 11, 2014
Published: August 19, 2014

photosensitizer is connected covalently to a catalytic metal center such as Pt and Pd via a conjugated bridge, which can mediate directional electron transfer. Several PS−B−C (PS, photosensitizer; B, bridge; C, catalytic center) model systems have been reported based on this strategy. Rau and co-workers reported a Pd-based complex that shows a maximum turnover number (TON) of 238 with 15 vol % water using TEA as sacrificial electron donor.[7,8] The fundamental photophysics of this compound have also been studied showing directional intramolecular electron transfer.[9,10] Sakai and co-workers have reported a series of Pt-based complexes, and the structure−activity relationship and reaction mechanism have been discussed.[11,12] Fihri and co-workers have reported several Co-based complexes, which also exhibit proton reduction to hydrogen.[13] Although a variety of complexes showing varying TONs have been reported, it should be noted that the hydrogen evolving conditions (e.g., sacrificial donor concentration, water percentage, irradiation intensity, pH value) are generally different in each case. In addition, the TONs obtained are the result of a sequence of photophysical and photochemical processes, so the photocatalytic performance cannot be judged from the reported TONs alone. However, by studying the fundamental photophysics of the complexes, it is possible to obtain a deeper insight into the systems, which is essential to establish routes for improvement.

Recently,[14] a new Ru−polypyridine−Pd complex (see Figure 1, **RuPd**) was reported, which shows a TON value of 130 over

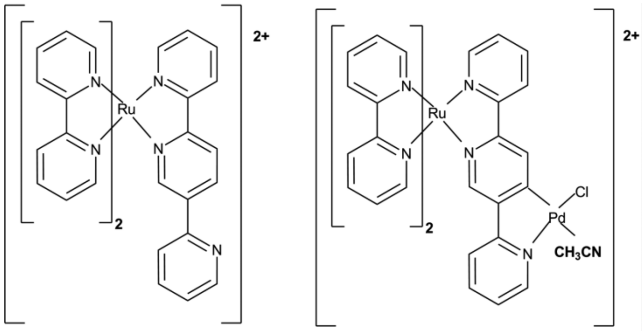

Figure 1. Molecular structure of **Ru** (left) and **RuPd** (right).

18 h of irradiation at 470 nm. Interestingly, a closely related Ru compound based on a 2,5-di(pyridin-2-yl)pyrazine bridging ligand was shown to be completely inactive with regard to photocatalytic hydrogen generation. This absence of photocatalytic activity has been assigned to fast quenching and absence of electron transfer to the Pt catalytic site.[12] Another closely related compound based on a 2,2′:6′,2″-terpyridine bridging ligand (instead of 2,2′:5′,2″-terpyridine) did not show any photocatalytic activity.[14] This inactivity is due to the short-lived excited state of the Ru chromophore (see Supporting Information, Figure S1, for the transient absorption data) and is therefore not investigated in more detail. The reason for the photocatalytic activity of the **RuPd** compound is not understood, and is explored in this work. This photophysical study is important since it will facilitate the design of improved electronic pathways for photocatalytic hydrogen generation.

In this contribution, the intramolecular electron transfer processes that take place following photoexcitation of the terpyridine based **RuPd** complex (Figure 1, right) are reported. Resonance Raman (RR) spectroscopy is used to probe the localization of the initial excited states in the Franck−Condon (FC) region.[15,16] The temporal evolution of these excited states is probed by ultrafast transient absorption (TA) spectroscopy, which provides kinetic information from the 100 fs to the subnanosecond time domain. The relaxation of the lowest excited states (in the ns domain) is studied by time-resolved photoluminescence (PL). Covering the complete time range over which the photophysical processes occur, a comparison of the behavior of the dinuclear **RuPd** complex with that of its mononuclear precursor **Ru** (Figure 1, left) allows us to identify the impact of the Pd center on the photophysics. We present evidence for photoinduced electron transfer from the Ru(II) center to both the peripheral bpy ligands and the bridging tpy ligand, and confirm the occurrence of an interligand (bpy → tpy) electron transfer process. In addition, we propose the presence of a vibrational relaxation loss channel on the bpy ligands, which competes with the interligand (bpy → tpy) electron transfer process. These insights are essential for the design of novel Ru-based photocatalytic complexes for efficient hydrogen generation.

EXPERIMENTAL SECTION

(1). Materials and Steady State Characterization. The synthesis of the polypyridyl Ru(II) complex **Ru** and its cyclometalated counterpart **RuPd** was described earlier.[14] ^{1}H NMR spectral data are provided as Supporting Information. The complexes were dissolved in acetonitrile (Sigma-Aldrich, purity >99.5%) in 1 cm path length quartz cuvettes for steady state measurements. UV−vis absorption spectra were recorded using a SHIMADZU UV-1800 spectrophotometer. Steady state emission spectra were obtained using a Horiba Jobin Yvon FluoroMax-4 spectrofluorometer with excitation at 450 nm, with the same optical density (OD) at the excitation wavelength for **Ru** and **RuPd**. Both absorption and emission spectra were recorded at room temperature.

(2). Resonance Raman Spectroscopy. Raman spectra were recorded at 473 nm (Cobolt Lasers 50 mW) in 1 cm path length quartz cuvettes. The excitation beam was focused at the sample using a 10 cm focal length parabolic mirror at ca. 35° with respect to the collection axis. The Raman scattering was collected and collimated with a 2.5 cm diameter, 15 mm focal length plano convex mirror, filtered to remove Rayleigh scattering using a Steep Edge long pass filter (Semrock), focused into a spectrograph (Shamrock 303, AndorTechnology, 1200 l/mm grating blazed at 500 nm), and imaged onto a Andor iDus-420-BEX2-DD CCD camera.

(3). Ultrafast Transient Absorption Spectroscopy. Samples for transient absorption (TA) experiments were prepared by dissolving the compounds in anhydrous acetonitrile (Sigma-Aldrich, purity >99.9%) in 1 mm optical path length quartz cuvettes. All samples had the same OD (0.45) at 480 nm (excitation wavelength). Photoinduced chemical degradation was excluded by comparison of the UV−vis absorption spectra recorded before and after the TA experiments.

The femtosecond TA system consists of an amplified Ti:sapphire laser system (Clark MXR CPA-2001), which produces laser pulses at 775 nm at 1 kHz repetition rate, with a pulse duration less than 120 fs. Part of this 775 nm output is directed into a noncollinear optical parametric amplifier (NOPA, Clark MXR), to generate a pump beam at 480 nm, and is compressed afterward by a SF10 prism pair, yielding a pulse duration around 50 fs, and a fwhm bandwidth of 7 nm. After compression, the pump beam is focused onto the

dx.doi.org/10.1021/jp506269h | J. Phys. Chem. C 2014, 118, 20799−20806

sample by using a parabolic mirror, and the beam diameter is about 250 μm.[17] The remaining part of the fundamental 775 nm beam, after passing a mechanical delay stage, is focused onto a 3 mm thick CaF_2 window (001-cut, Newlight Photonics Inc.) to generate a white light continuum (345−700 nm), which is used as the probe. The CaF_2 crystal is mounted on a continuously moving stage to avoid thermal damage. The polarization angle between the pump and probe beams is set at magic angle (54.7°).[4] The pulse energy of the pump was ca. 1.5 $\times 10^{-4}$ J/cm^2 (3.7×10^{14} photons/cm^2), and was verified to be in the linear regime. After passing through the sample, the pump beam is blocked and the probe beam is spectrally dispersed using a spectrograph (Acton SP-150, 150 grooves/mm grating). A photodiode array consisting of 256 pixels is used to record the data.

TA data were numerically corrected for chirp by fitting the spectral-temporal traces of pure solvent coherent artifact peaks with a polynomial function, and by subsequent correction of the time axis based on that polynomial function. From the coherent artifact signals, the TA time resolution was determined to be 100−150 fs. The open-source software Glotaran[18] was used for data analysis.

(4). Time-Resolved Photoluminescence. Samples were prepared in a similar way as in the UV−vis absorption experiments, and were degassed using N_2 gas. Time-resolved photoluminescence was measured using a FluoroMax Spectrofluorometer extended for time-correlated single photon counting measurements (HORIBA JOBIN YVON, FluoroMax-4 TCSPC). A NanoLED-460 laser source (462 nm, 1.3 ns pulse duration) was used to excite the samples at 250 kHz repetition rate. The emission lifetime data were taken at 635 nm for both **Ru** and **RuPd**.

RESULTS AND DISCUSSION

(1). Steady State Characterization. The absorption and emission spectra of **Ru** and **RuPd** (Figure 2) exhibit metal-to-ligand charge transfer (^{1}MLCT) absorption bands between 400 and 550 nm (maxima at 446 nm for **Ru** and 462 nm for **RuPd**).[2,5,19,20] Excitation at 480 nm allows sufficient TA signal amplitude and at the same time minimizes vibration and solvent relaxation from the Franck−Condon region to the THEXI (thermally equilibrated excited states), and has therefore been chosen as the pump wavelength in the TA experiments (vide infra). The absorption bands at ca. 280 nm for **Ru** and 290 nm for **RuPd** correspond to the bpy ligand centered (LC) $\pi-\pi^*$ transitions,[19,21] and the shoulders at ca. 300 nm for **Ru** and 310 nm for **RuPd** have been assigned earlier[14] to the tpy ligand based $\pi-\pi^*$ transitions on the basis of resonance Raman spectroscopy. The shift to longer wavelength for these latter bands compared with those of bpy is due to the increased conjugation present in tpy ligands.

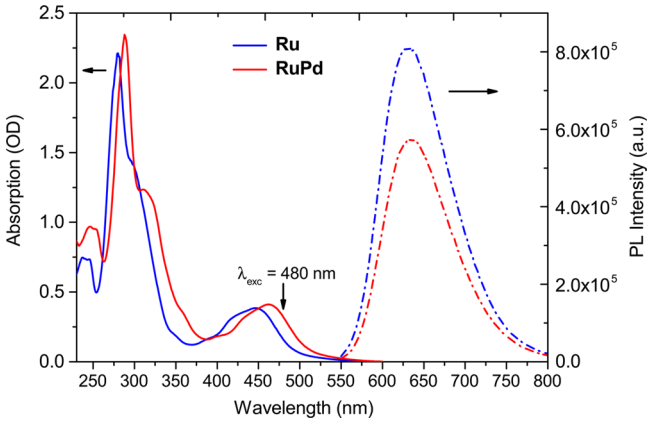

Figure 2. Steady state UV−vis absorption (solid lines) and photoluminescence (dashed dot lines) of **Ru** (blue) and **RuPd** (red).

The emission at ca. 635 nm is typical for radiative relaxation from the lowest ^{3}MLCT states to the ground state. The ^{3}MLCT states are generally described as a manifold of thermally equilibrated excited states with varying degrees of triplet character for Ru(II) polypyridyl complexes.[19,22,23] The emission of both **Ru** and **RuPd** are comparable in terms of spectral shape and quantum yield (0.047 for **Ru** and 0.032 for **RuPd**[14]), indicating that the energy gap between the lowest ^{3}MLCT and the ground state is not substantially perturbed by the presence of Pd(II). A decrease in emission lifetime is observed on going from **Ru** to **RuPd** (see discussion below).

(2). Localization of the Initial ^{1}MLCT Transitions. Resonance Raman spectroscopy has been demonstrated to be a powerful tool to study the wave packet motion in the Franck−Condon region.[9,16,24] Hence, identification of the various vibrational modes with strong resonance enhancement provides information about the localization of the initial excited states upon optical excitation. This information is complementary to the results obtained from TA, which has a time resolution of 100−150 fs.

Raman spectra of **Ru**, **RuPd** and $[Ru(bpy)_3]^{2+}$ recorded in acetonitrile are shown in Figure 3. The peak positions are listed in Table 1. At λ_{exc} 473 nm, which is close to the pump wavelength (480 nm) used in the TA experiments, the Raman scattering from the ligands associated with the ^{1}MLCT ← GS (GS: ground state) transitions are enhanced through resonance.

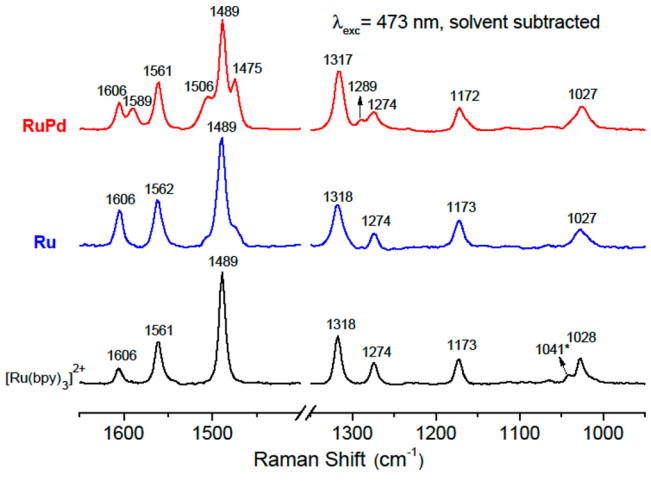

Figure 3. Raman spectra of **Ru** (blue), **RuPd** (red) and $[Ru(bpy)_3]^{2+}$ (black) in acetonitrile (ca. 0.1 mM, solvent contributions have been removed by scaled subtraction) recorded at λ_{exc} 473 nm. The band at 1041 cm^{-1} (∗) in the last spectrum is due to imperfect subtraction of the solvent signal.

In all three spectra, the characteristic modes of $[Ru(bpy)_3]^{2+}$ are apparent consistent with resonance with ^{1}MLCT(t_2-Ru(II) to π^*-bpy) transitions at 473 nm. Resonance with ^{1}MLCT(t_2-Ru(II) to π^*-tpy) transition is also observed for **Ru**, in particular at 1606, ∼1507, ∼1473, and 1318 cm^{-1}. In the case of **RuPd**, additional tpy associated mode are observed at 1589

dx.doi.org/10.1021/jp506269h | J. Phys. Chem. C 2014, 118, 20799−20806

Table 1. Comparison of Raman Bands [cm^{-1}] of Ru and RuPd with Those of $[Ru(bpy)_3]^{2+}$

$[Ru(bpy)_3]^{2+}$	Ru	RuPd
1028	1027	1027
1173	1173	1172
1274	1274	1274
–	–	1289
1318	1318	1317
–	–	1475
1489	1489	1489
–	–	1506
1561	1562	1561
–	–	1589
1606	1606	1606

cm^{-1} under the influence of Pd coordination. Note that some tpy and bpy associated modes overlap at 1606 and 1318 cm^{-1}. The assignment of the Raman bands based on deuteration experiments is given in Supporting Information S3. In conclusion, resonance Raman confirms the initial population of both bpy and tpy based ^{1}MLCT states in **Ru** and **RuPd** upon excitation at 473 nm.

(3). Transient Absorption in the Femto- and Picosecond Time Domain. The subsequent dynamics that take place after photoexcitation in the femto- and picosecond time domain have been probed by time-resolved TA spectroscopy. Figure 4A shows the TA spectra of **Ru** at several delay times between pump and probe pulses, together with the kinetic traces (ΔOD vs time) at key wavelengths plotted in Figure 4B. Although spectral changes are observed in the region above 500 nm (related to ^{3}LMCT (ligand-to-metal charge transfer) transitions[25]), the most informative time dependent changes are observed in the blue-UV region, with two pronounced bands at ca. 370 and 420 nm. The former is assigned to the excited state absorption (ESA) of the bpy^- monoanion ($\pi^{**} \leftarrow \pi^*$, intraligand),[25,26] while the latter is assigned to the ESA of the tpy^- monoanion ($\pi^{**} \leftarrow \pi^*$, intraligand).[27,28] Notably, the ground state bleach (GSB) signal at ca. 450 nm shows no significant change between 500 fs and 500 ps.

At 500 fs, the intensities of the ESA bands at 370 and 420 nm are comparable. Between 500 fs and 20 ps a decrease in the absorption at 370 nm (associated with the bpy^- monoanion) and an increase in the absorption at 420 nm (associated with the tpy^- monoanion) are observed, with an isosbestic point maintained at ca. 375 nm. After ca. 20 ps, the TA spectra show no significant change until at least 500 ps, indicating that the system is in a fully relaxed excited state. The absence of any significant change in the GSB signal over time indicates that the process observed involves interligand (from the bpy-localized ^{3}MLCT state to the tpy-localized ^{3}MLCT state) electron transfer, and is not due to recombination to the ground state. Furthermore, the observation of the bpy^- based ESA at 370 nm even after 500 ps indicates that the bpy^- monoanion is present even after finalization of the interligand charge transfer process, suggesting a competing relaxation channel which is localized on the bpy ligand. This observation is consistent with the nanosecond transient Raman spectroscopy studies reported earlier, which showed the presence of characteristic features (1210 and 1282 cm^{-1}) of the bpy anion radical.[14] The possibility of solvated electrons is excluded, as the ESA bands in the 500−700 nm region do not show the characteristic solvated dimer anion features in the picosecond time domain.[29] The above interpretation will be referred to as the interligand electron transfer model in further discussion. This interpretation is consistent with an earlier work reporting interligand electron transfer in a Ru(II)-polypyridyl complex on TiO_2 occurring on a ps time scale.[35]

Alternatively, the observed TA features can be interpreted as the result of an interligand equilibration process between the $^3MLCT_{bpy}$ and $^3MLCT_{tpy}$ excited states. Note that in this case, the interligand electron transfer occurs not only from bpy to tpy, but also vice versa possibly through thermal activation. The relaxation from the Franck−Condon region (i.e., arising from a mixture of the $^1MLCT_{bpy}$ and $^1MLCT_{tpy}$ states) does not immediately lead to a thermally equilibrated situation into the ^{3}MLCT manifolds. Instead, equilibration (of the electron density over the bpy and tpy ligands) occurs over ca. 20 ps. This interpretation will be referred as the equilibration model in further discussion.

The TA spectra for **RuPd** are shown in Figure 5A and the kinetic traces at selected wavelengths are plotted in Figure 5B. The most notable difference between the TA spectra of **Ru** and **RuPd** is that the tpy^- associated ESA band at 420 nm is much less intense for the latter, while the intensities of the bpy^- associated ESA band at 370 nm and the GSB signal are comparable. The less intense absorption around 420 nm could be caused by a decrease in oscillator strength of the tpy^- associated ESA band due to the close proximity of the Pd atom.

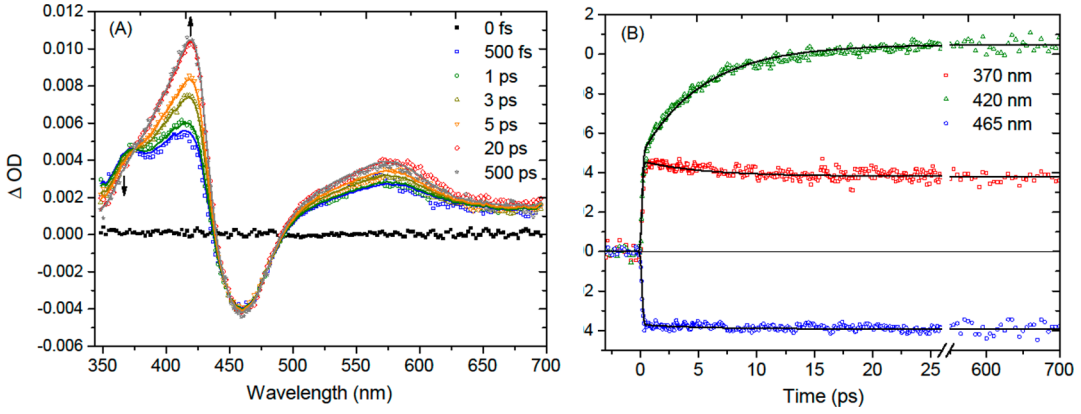

Figure 4. TA spectra of **Ru** (A) and corresponding kinetic traces at selected wavelengths (B). The fits based on a target analysis model (vide infra) are represented by solid curves.

dx.doi.org/10.1021/jp506269h | J. Phys. Chem. C 2014, 118, 20799−20806

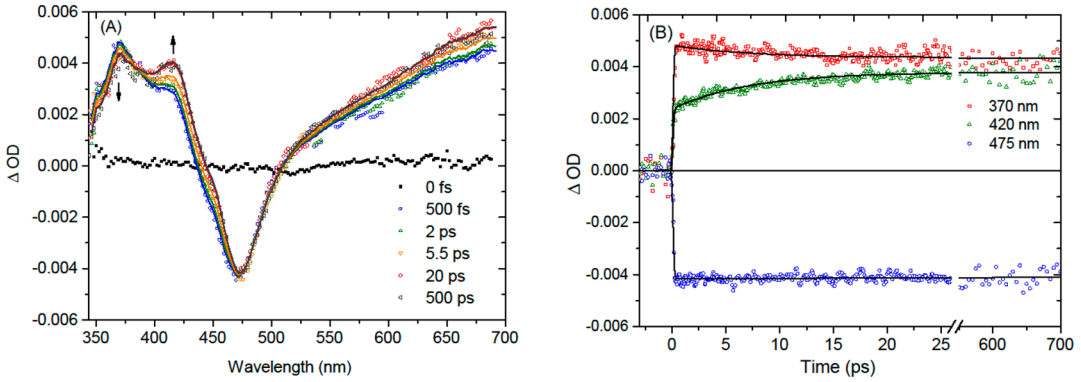

Figure 5. TA spectra of **RuPd** (A) and corresponding kinetic traces at selected wavelengths (B). The fits based on a target analysis model (vide infra) are represented by solid curves.

Alternatively, this phenomenon may be due to charge delocalization over the tpy ligand and the Pd center. Interestingly, the kinetic trace at 370 nm of **RuPd** (Figure 5B) associated with the bpy ligand remains similar compared to that of **Ru** (Figure 4B). This observation suggests that the degree of electron transfer from bpy to tpy is comparable for **Ru** and **RuPd**, presuming that the oscillator strength of the bpy^- associated ESA band at 370 nm is not significantly affected by the Pd center coordinated to the tpy ligand. A second difference between the TA spectra of **Ru** and **RuPd** is that the broad ESA bands in the longer wavelength region (500−700 nm) are red-shifted for **RuPd**. This difference is most likely due to the influence of Pd on the ^{3}LMCT transitions from the tpy ligand to the formerly oxidized Ru(III) center.

Similar to **Ru**, between 500 fs and 20 ps, a decrease in absorbance at 370 nm and an increase in absorbance at 420 nm is observed, with an isosbestic point at ca. 385 nm. The TA spectrum remains constant between 20 and 500 ps, indicating that the interligand (from bpy to tpy) electron transfer process (or the equilibration between the $^3MLCT_{bpy}$ and $^3MLCT_{tpy}$ excited states) is completed within ca. 20 ps, and recombination to the ground state is insignificant at this time scale. Note that the bpy^- associated ESA band at 370 nm does not decrease further after 20 ps, indicating that the bpy ligands remain reduced to a certain degree, consistent with the observation of the characteristic bpy anion radical Raman bands in the ns-transient Raman spectrum of the complex.[14]

(4). Relaxation of the ^{3}MLCT States in the Nanosecond Domain. TA spectroscopy shows the presence of long-lived relaxed ^{3}MLCT states, whose decays have been studied by nanosecond time-resolved photoluminescence (PL). Figure 6 shows the PL decays of **Ru** and **RuPd**. The PL decay of **Ru** can be described with a monoexponential decay function with a time constant of 623 (±1) ns. The PL decay of **RuPd** is biexponential and can be described using time constants of 88 (±1) ns and 400 (±1) ns, with the faster component dominating (62%).

The monoexponential decay observed for **Ru** indicates that both the relaxed $^3MLCT_{bpy}$ and $^3MLCT_{tpy}$ states decay with time constants close to 623 ns. For **RuPd**, however, the observed biexponential decay indicates that the relaxed $^3MLCT_{bpy}$ and $^3MLCT_{tpy}$ states decay with different time constants. The 88 ns component is assigned to the emission from the $^3MLCT_{tpy}$ state to the ground state, as coupling to Pd is likely to decrease the excited state lifetime due to the

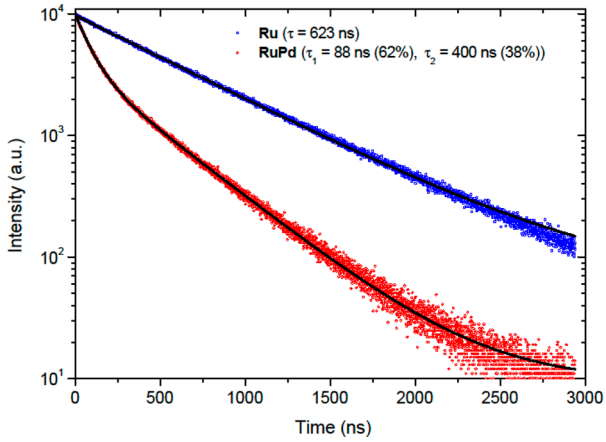

Figure 6. Time-resolved PL decay (at 635 nm) of **Ru** (blue) and **RuPd** (red) obtained on excitation at 460 nm. Fits to a monoexponential (**Ru**) and biexponential decay (**RuPd**) are represented by black solid lines, and the obtained time constants are included.

presence of an additional decay channel (electron transfer from tpy to Pd) and/or due to a more efficient radiative decay pathway as a result of spin−orbital coupling. The 400 ns component is attributed to the emission from the $^3MLCT_{bpy}$ state to the ground state, as the bpy ligand is relatively far from the Pd center and is therefore less affected.

The faster PL decay of the $^3MLCT_{tpy}$ state in **RuPd** allows estimation of the electron transfer time from the tpy ligand to the Pd(II) center, which is longer than 88 ns.[30] Compared to the interligand electron transfer process (from bpy to tpy) occurring on the picosecond time scale, the electron transfer from the tpy ligand to Pd(II) seems to occur much slower in the nanosecond time domain. Notably, a much faster bridge-Pd electron transfer time (310 ps) has been reported before[9] for another Ru−Pd based complex.

It is also possible that the tpy based excited state is delocalized over the Pd(II) moiety and the tpy ligand, and this delocalization reduces the ESA band (420 nm) brightness in the TA spectra of **RuPd** as compared to **Ru**. In this case, the shorter $^3MLCT_{tpy}$ lifetime for **RuPd** compared to **Ru** is caused mainly by a more efficient radiative decay pathway, rather than directional electron transfer to the Pd center. The nonradiative decay pathway may become less dominant, as Pd likely increases the rigidity of the complex. This is supported by the observation for a platinated Ru complex reported by Sakai and

dx.doi.org/10.1021/jp506269h | J. Phys. Chem. C 2014, 118, 20799−20806

co-workers.[31] In their case, the Ru−Pt dimer has an even longer PL lifetime than the Ru monomer, which is ascribed to an increase in ligand rigidity upon platination.

(5). Photophysical Modeling. Resonance Raman data show that optical excitation leads to population of both the $^1MLCT_{bpy}$ and $^1MLCT_{tpy}$ manifolds. This is supported by the observation of ESA bands at both 370 and 420 nm in the TA spectra at 200 fs (see Supporting Information, Figure S4). ISC in $[Ru(bpy)_3]^{2+}$ is known to occur on a time scale of ∼100 fs or even faster in acetonitrile.[3−5,25] We assume that ISC processes are similarly fast in **Ru** and **RuPd**, and that the $^3MLCT_{bpy}$ and $^3MLCT_{tpy}$ triplet states are formed within the TA instrumental response time of 100−150 fs. Vibrational cooling after ISC is known to occur on a ps time scale.[23,25,32] This process is accompanied by interligand electron transfer from the bpy ligands to the tpy ligand within ca. 20 ps, as discussed in the previous section. Importantly, the presence of the bpy^- associated ESA band at 370 nm after 20 ps indicates that not all electron density moves toward the tpy ligand. This phenomenon is likely due to a loss channel associated with the bpy ligand competing with the interligand electron transfer process (interligand electron transfer model). An alternative explanation involves an excited state interligand equilibration process between the $^3MLCT_{bpy}$ and $^3MLCT_{tpy}$ manifolds (equilibration model). Equilibration is known in literature for intraligand electron transfer process in a Ru complex[33] but to our knowledge has not been reported for interligand interactions in Ru complexes. The interpretation based on interligand electron transfer is most consistent with existing literature (vide infra) and therefore chosen for target analysis.

The photophysical model used for target analysis is shown in Figure 7. Optical excitation leads to population of both the bpy- and tpy-based ^1MLCT states, followed by ultrafast ISC processes within the instrumental response time (100−150 fs). The population percentage of the bpy-based and tpy-based ^3MLCT triplet states is determined by inspecting the shape and position of the obtained species associated spectra (SAS, vide infra). Two distinct bpy-based ^3MLCT states are distinguished, one is assigned to a hot $^3MLCT_{bpy}$ state and the other to a relaxed state; interligand electron transfer to the tpy ligand is possible only from the hot $^3MLCT_{bpy}$ state. The absorption spectra of the hot and relaxed $^3MLCT_{bpy}$ states are assumed to be identical. Both ISC from the $^1MLCT_{tpy}$ state and interligand electron transfer from the bpy ligand lead to the population of the $^3MLCT_{tpy}$ state. The time scales for cooling of the hot bpy-based ^3MLCT state and interligand electron transfer are obtained by fitting the model to the TA data. The decay time constants of the relaxed ^3MLCT states to the ground state are obtained from the emission lifetime values. Note that this photophysical model is not the only model that can describe the observed TA spectra; the model based on equilibration between the $^3MLCT_{bpy}$ and $^3MLCT_{tpy}$ manifolds is also capable of fitting the TA data.

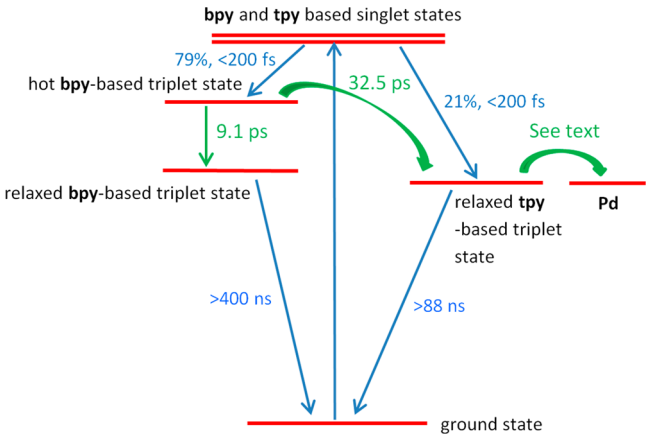

Figure 7. Simplified photophysical model for light-induced processes in **RuPd**.

Figure 8 shows the SAS of **RuPd** based on the model presented in Figure 7, with the scaled and inverted steady state absorption spectrum included as a gray area (the SAS of **Ru** is provided in Figure S5 of the Supporting Information). The SAS associated with the bpy ligand combined with the GSB signal (Figure 8, blue curve) resembles the TA spectrum of $[Ru(bpy)_3]^{2+}$ published earlier.[25] Note that the steady state absorption of **RuPd** is red-shifted compared to that of $[Ru(bpy)_3]^{2+}$. The SAS associated with the tpy ligand combined with the GSB signal (Figure 8, red curve) is positive around 450 nm due to the ESA(tpy^-) contribution in this region. The LMCT bands (above 500 nm) associated with the tpy ligand are more intense than those associated with the bpy ligand, both for **RuPd** (Figure 8) and **Ru** (Supporting Information, Figure S5). The coupling between the tpy ligand and the Pd(II) center may lead to a strong LMCT absorption in this region.

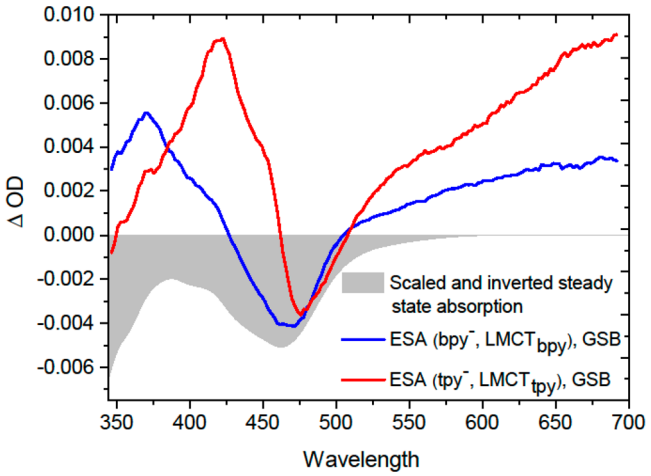

Figure 8. Species-associated spectra (SAS) of **RuPd**. The gray area represents the scaled and inverted steady state absorption spectrum.

The obtained interligand electron transfer time equals 8.8 (±0.7) ps for **Ru** and 32.5 (±1.5) ps for **RuPd**. These values are close to the ∼20 ps found by Sundström and co-workers for a Ru(II)-based photosensitizer on TiO_2.[35] The competing bpy-localized loss process has a time constant of 13.4 (±1.5) ps for **Ru** and 9.1 (±0.4) ps for **RuPd**. It appears that coordinating Pd to the tpy ligand slows down the interligand electron transfer process. However, the competing bpy-localized loss process does not slow down much when coupling Pd to tpy. This competing process is very likely to be assigned to the vibrational relaxation of bpy, which is reported to be 5−15 ps by various groups.[23,25,32] It is difficult to rationalize why coupling to Pd slows down the interligand electron transfer process. One possible reason is that this process is coupled to the rotation of the complex and/or vibration of the tpy ligand.

dx.doi.org/10.1021/jp506269h | J. Phys. Chem. C 2014, 118, 20799−20806

TA anisotropy measurements have demonstrated a rotational decay constant of about 40−50 ps for $[Ru(bpy)_3]^{2+}$ in acetonitrile at room temperature.[25,34] As Pd likely slows down molecular rotation and increases the rigidity of the tpy ligand, interligand electron transfer may become slower and as a result less competitive to the vibrational cooling of bpy. Note that the extracted time constant of 32.5 (±1.5) ps also includes possible vibrational relaxation processes within tpy. As spectral narrowing features are not observed in this time range, information regarding the cooling process of tpy has not been extracted.

CONCLUSION

Optical excitation of **Ru** and **RuPd** leads to the population of both bpy- and tpy-based ^{1}MLCT states, followed by ISC into corresponding hot ^{3}MLCT states. Electron density localized on the bpy ligand can subsequently flow to the tpy ligand (interligand electron transfer process), which is finalized within 20 ps. The electron density does not entirely end up on the tpy ligand, but partially remains on the bpy ligand, most likely due to a competing loss channel related to vibrational relaxation of the bpy ligand. For efficient hydrogen evolution, it is essential to make interligand electron transfer faster. One possible approach to realize this involves functionalizing the peripheral ligands with electron-donating moieties. Other important parameters involve the nature of the bridging ligand, and the catalytic metal center.

A second aspect to address is the localization of the electron density after the interligand electron transfer process. Electron transfer from tpy to Pd may occur on a time scale of ∼100 ns. This process competes with the decay of the $^3MLCT_{tpy}$ state to the ground state, which limits the practical hydrogen evolving applications. Alternatively, the electron may populate a hybrid orbital formed between tpy and Pd. In the latter case, it is needed to extend the lifetime of this state as long as possible, as the tpy bridging ligand and the Pd center together act as a hybrid electron storage unit. X-ray transient absorption will be performed in the near future for further investigation.[36]

ASSOCIATED CONTENT

Supporting Information

NMR, additional TA and resonance Raman spectra, and SAS of **Ru**. This material is available free of charge via the Internet at http://pubs.acs.org

AUTHOR INFORMATION

Corresponding Author

*(A.H.) E-mail: j.m.huijser@utwente.nl.

Author Contributions

The manuscript was written through contributions of all authors. All authors have given approval to the final version of the manuscript.

Notes

The authors declare no competing financial interest.

ACKNOWLEDGMENTS

This work is supported by the Dutch Organization for Scientific Research (NWO), and the Sector Plan Physics and Chemistry, the European Research Council (Consolidator Investigator Grant no. 279549, WRB, FM) and Funding from the Ministry of Education, Culture and Science (Gravity program 024.001.035, WRB). Prof. Villy Sundström from Lund University in Sweden is acknowledged for scientific discussions.

REFERENCES

(1) Armaroli, N.; Balzani, V. The future of energy supply: Challenges and opportunities. *Angew. Chem., Int. Ed.* **2007**, *46*, 52−66.

(2) Juris, A.; Balzani, V.; Barigelletti, F.; Campagna, S.; Belser, P.; Vonzelewsky, A. Ru(II) polypyridine complexes - photophysics, photochemistry, electrochemistry, and chemi-luminescence. *Coord. Chem. Rev.* **1988**, *84*, 85−277.

(3) Damrauer, N. H.; Cerullo, G.; Yeh, A.; Boussie, T. R.; Shank, C. V.; McCusker, J. K. Femtosecond dynamics of excited-state evolution in $[Ru(bpy)_3]^{2+}$. *Science* **1997**, *275*, 54−57.

(4) Yeh, A. T.; Shank, C. V.; McCusker, J. K. Ultrafast electron localization dynamics following photo-induced charge transfer. *Science* **2000**, *289*, 935−938.

(5) Cannizzo, A.; van Mourik, F.; Gawelda, W.; Zgrablic, G.; Bressler, C.; Chergui, M. Broadband femtosecond fluorescence spectroscopy of $[Ru(bpy)_3]^{2+}$. *Angew. Chem., Int. Ed.* **2006**, *45*, 3174−3176.

(6) Halpin, Y.; Pryce, M. T.; Rau, S.; Dini, D.; Vos, J. G. Recent progress in the development of bimetallic photocatalysts for hydrogen generation. *Dalton Trans.* **2013**, *42*, 16243−16254.

(7) Rau, S.; Schafer, B.; Gleich, D.; Anders, E.; Rudolph, M.; Friedrich, M.; Gorls, H.; Henry, W.; Vos, J. G. A supramolecular photocatalyst for the production of hydrogen and the selective hydrogenation of tolane. *Angew. Chem., Int. Ed.* **2006**, *45*, 6215−6218.

(8) Karnahl, M.; Kuhnt, C.; Ma, F.; Yartsev, A.; Schmitt, M.; Dietzek, B.; Rau, S.; Popp, J. Tuning of photocatalytic hydrogen production and photoinduced intramolecular electron transfer rates by regioselective bridging ligand substitution. *ChemPhysChem* **2011**, *12*, 2101−2109.

(9) Tschierlei, S.; Presselt, M.; Kuhnt, C.; Yartsev, A.; Pascher, T.; Sundström, V.; Karnahl, M.; Schwalbe, M.; Schafer, B.; Rau, S.; Schmitt, M.; Dietzek, B.; Popp, J. Photophysics of an intramolecular hydrogen-evolving Ru-Pd photocatalyst. *Chem.—Eur. J.* **2009**, *15*, 7678−7688.

(10) Tschierlei, S.; Karnahl, M.; Presselt, M.; Dietzek, B.; Guthmuller, J.; Gonzalez, L.; Schmitt, M.; Rau, S.; Popp, J. Photochemical fate: the first step determines efficiency of H_2 formation with a supramolecular photocatalyst. *Angew. Chem., Int. Ed.* **2010**, *49*, 3981−3984.

(11) Ozawa, H.; Yokoyama, Y.; Haga, M.; Sakai, K. Syntheses, characterization, and photo-hydrogen-evolving properties of tris(2,2′-bipyridine) ruthenium(II) derivatives tethered to a cis-Pt(II)Cl_2 unit: insights into the structure-activity relationship. *Dalton Trans.* **2007**, 1197−1206.

(12) Ozawa, H.; Sakai, K. Photo-hydrogen-evolving molecular devices driving visible-light-induced water reduction into molecular hydrogen: structure-activity relationship and reaction mechanism. *Chem. Commun.* **2011**, *47*, 2227−2242.

(13) Fihri, A.; Artero, V.; Razavet, M.; Baffert, C.; Leibl, W.; Fontecave, M. Cobaloxime-based photocatalytic devices for hydrogen production. *Angew. Chem., Int. Ed.* **2008**, *47*, 564−567.

(14) Bindra, G. S.; Schulz, M.; Paul, A.; Groarke, R.; Soman, S.; Inglis, J. L.; Browne, W. R.; Pfeffer, M. G.; Rau, S.; MacLean, B. J.; Pryce, M. T.; Vos, J. G. The role of bridging ligand in hydrogen generation by photocatalytic Ru/Pd assemblies. *Dalton Trans.* **2012**, *41*, 13050−13059.

(15) Heller, E. J.; Sundberg, R. L.; Tannor, D. Simple aspects of Raman-scattering. *J. Phys. Chem.* **1982**, *86*, 1822−1833.

(16) Wachtler, M.; Guthmuller, J.; Gonzalez, L.; Dietzek, B. Analysis and characterization of coordination compounds by resonance Raman spectroscopy. *Coord. Chem. Rev.* **2012**, *256*, 1479−1508.

(17) Savolainen, J.; van der Linden, D.; Dijkhuizen, N.; Herek, J. L. Characterizing the functional dynamics of zinc phthalocyanine from femtoseconds to nanoseconds. *J. Photochem. Photobiol. A* **2008**, *196*, 99−105.

(18) Snellenburg, J. J.; Laptenok, S. P.; Seger, R.; Mullen, K. M.; van Stokkum, I. H. M. Glotaran: A Java-based graphical user interface for the R package TIMP. *J. Stat. Softw.* **2012**, *49*, 1−22.

(19) Kalyanasundaram, K. Photophysics, photochemistry and solar-energy conversion with tris(bipyridyl)ruthenium(II) and its analogs. *Coord. Chem. Rev.* **1982**, *46*, 159−244.
(20) Daul, C.; Baerends, E. J.; Vernooijs, P. A density-functional study of the MLCT states of $[Ru(bpy)_3]^{2+}$ in D_3 symmetry. *Inorg. Chem.* **1994**, *33*, 3538−3543.
(21) Heath, G. A.; Yellowlees, L. J.; Braterman, P. S. Spectroelectrochemical studies on tris-bipyridyl ruthenium complexes; ultraviolet, visible, and near-infrared spectra of the series $[Ru(bipyridyl)_3]^{2+/1+/0/1-}$. *J. Chem. Soc. Chem. Commun.* **1981**, 287−289.
(22) Sauvage, J. P.; Collin, J. P.; Chambron, J. C.; Guillerez, S.; Coudret, C.; Balzani, V.; Barigelletti, F.; Decola, L.; Flamigni, L. Ruthenium(II) and osmium(II) bis(terpyridine) complexes in covalently-linked multicomponent systems: synthesis, electrochemical behavior, absorption spectra, and photochemical and photophysical properties. *Chem. Rev.* **1994**, *94*, 993−1019.
(23) Henry, W.; Coates, C. G.; Brady, C.; Ronayne, K. L.; Matousek, P.; Towrie, M.; Botchway, S. W.; Parker, A. W.; Vos, J. G.; Browne, W. R.; McGarvey, J. J. The early picosecond photophysics of Ru(II) polypyridyl complexes: a tale of two timescales. *J. Phys. Chem. A* **2008**, *112*, 4537−4544.
(24) Heinze, K.; Hempel, K.; Tschierlei, S.; Schmitt, M.; Popp, J.; Rau, S. Resonance Raman studies of bis(terpyridine)ruthenium(II) amino acid esters and diesters. *Eur. J. Inorg. Chem.* **2009**, 3119−3126.
(25) Wallin, S.; Davidsson, J.; Modin, J.; Hammarström, L. Femtosecond transient absorption anisotropy study on $[Ru(bpy)_3]^{2+}$ and $[Ru(bpy)(py)_4]^{2+}$. Ultrafast interligand randomization of the MLCT state. *J. Phys. Chem. A* **2005**, *109*, 4697−4704.
(26) Krejcik, M.; Vlcek, A. A. Electrochemical formation of dianions of 2,2′-bipyridine and related compounds. *J. Electroanal. Chem.* **1991**, *313*, 243−257.
(27) Hewitt, J. T.; Concepcion, J. J.; Damrauer, N. H. Inverse kinetic isotope effect in the excited-state relaxation of a Ru(II)-aquo complex: revealing the impact of hydrogen-bond dynamics on nonradiative decay. *J. Am. Chem. Soc.* **2013**, *135*, 12500−12503.
(28) Hewitt, J. T.; Vallett, P. J.; Damrauer, N. H. Dynamics of the ^{3}MLCT in Ru(II) terpyridyl complexes probed by ultrafast spectroscopy: evidence of excited-state equilibration and interligand electron transfer. *J. Phys. Chem. A* **2012**, *116*, 11536−11547.
(29) Doan, S. C.; Schwartz, B. J. Ultrafast studies of excess electrons in liquid acetonitrile: revisiting the solvated electron/solvent dimer anion equilibrium. *J. Phys. Chem. B* **2013**, *117*, 4216−4221.
(30) The electron transfer rate constant can be estimated from the equation $\tau_{\mathbf{RuPd}} = 1/(k_r + k_{nr} + k_{et}) = 88\ (\pm 1)$ ns, where τ_{RuPd} is the excited state lifetime of **RuPd**, and k_r, k_{nr}, and k_{et} represent the rate constants of radiative, nonradiative and electron transfer, respectively. Note that for **Ru**, the emission lifetime is determined only by radiative and nonradiative decay pathways.
(31) Sakai, K.; Ozawa, H.; Yamada, H.; Tsubomura, T.; Hara, M.; Higuchi, A.; Hagac, M. A. A tris(2,2 ′-bipyridine)ruthenium(II) derivative tethered to a cis-$PtCl_2$(amine)$_2$ moiety: syntheses, spectroscopic properties, and visible-light-induced scission of DNA. *Dalton Trans.* **2006**, 3300−3305.
(32) Damrauer, N. H.; McCusker, J. K. Ultrafast dynamics in the metal-to-ligand charge transfer excited-state evolution of $[Ru(4,4'$-diphenyl-2,2′-bipyridine$)_3]^{2+}$. *J. Phys. Chem. A* **1999**, *103*, 8440−8446.
(33) Brennaman, M. K.; Meyer, T. J.; Papanikolas, J. M. $[Ru(bpy)_2dppz]^{2+}$ light-switch mechanism in protic solvents as studied through temperature-dependent lifetime measurements. *J. Phys. Chem. A* **2004**, *108*, 9938−9944.
(34) Malone, R. A.; Kelley, D. F. Interligand electron transfer and transition state dynamics in Ru(II)trisbipyridine. *J. Chem. Phys.* **1991**, *95*, 8970−8976.
(35) Benkö, G.; Kallioinen, J.; Myllyperkiö, P.; Trif, F.; Korppi-Tommola, J. E. I.; Yartsev, A. P.; Sundström, V. Interligand electron transfer determines triplet excited state electron injection in RuN_3-sensitized TiO_2 films. *J. Phys. Chem. B* **2004**, *108*, 2862−2867.
(36) Canton, S. E.; Zhang, X. Y.; Zhang, J. X.; van Driel, T. B.; Kjaer, K. S.; Haldrup, K.; Chabera, P.; Harlang, T.; Suarez-Alcantara, K.; Liu, Y. Z.; Perez, J.; Bordage, A.; Papai, M.; Vanko, G.; Jennings, G.; Kurtz, C. A.; Rovezzi, M.; Glatzel, P.; Smolentsev, G.; Uhlig, J.; Dohn, A. O.; Christensen, M.; Galler, A.; Gawelda, W.; Bressler, C.; Lemke, H. T.; Møller, K. B.; Nielsen, M. M.; Lomoth, R.; Warnmark, K.; Sundström, V. Toward Highlighting the Ultrafast Electron Transfer Dynamics at the Optically Dark Sites of Photocatalysts. *J. Phys. Chem. Lett.* **2013**, *4*, 1972−1976.